JOURNAL OF AIRCRAFT
Vol. 32, No. 3, May–June 1995

Comparison of the Predictive Capabilities of Several Turbulence Models

Christopher L. Rumsey* and Veer N. Vatsa†
NASA Langley Research Center, Hampton, Virginia 23681

Four turbulence models are evaluated for transonic separated flows using two well-established solvers, one upwind and one central difference. The equilibrium model of Baldwin-Lomax predicts separated-flow shock locations too far aft. The effects of several modifications to the half-equation model of Johnson-King are explored in detail, and different versions of the model are compared. Good results for two- and three-dimensional flows can be obtained using two different versions of this model. The one-equation models of Baldwin-Barth and Spalart-Allmaras perform well for airfoil flows, but can predict the shock too far forward at the outboard stations of a separated wing. The effects of numerical truncation error are assessed using grid-refinement studies in combination with varying the numerical dissipation levels in both codes.

Introduction

As computational fluid dynamics (CFD) grows in capability as a tool for the analysis of three-dimensional aerospace configurations, turbulence modeling continues to be one of the primary factors that inhibits more widespread usage of Navier-Stokes codes by aircraft manufacturers. The search for a model that accurately predicts both attached and separated three-dimensinal flowfields is complicated by the fact that it is difficult to assess the capabilities of new or refined turbulence models because of inherent limitations in the CFD codes that use them.

Particularly relevant is the issue of truncation error; the density of the grid used, the type of differencing scheme employed, and, for central-difference schemes, the amount of artificial dissipation added for numerical stability are all likely to have an effect on the solution. By conducting a broad study that covers both two- and three-dimensional configurations and using grid refinement studies with more than one computer code, the effects of truncation error can be determined. Hence, a more accurate assessment of the turbulence models is possible.

This article assesses the predictive capabilities of several turbulence models for transonic flow over the ONERA M6 wing[1] and the Lockheed Wing C.[2] Two widely used computer codes, CFL3D[3] and TLNS3D,[4] are employed. Each of these codes can employ either the Baldwin-Lomax[5] or the Johnson-King[6] turbulence model. Additionally, CFL3D can employ the Baldwin-Barth[7] or the Spalart-Allmaras[8] turbulence model. To provide a wider basis for assessment, the capabilities of the various turbulence models are examined in two dimensions using the two-dimensional mode of CFL3D as well.

Presented as Paper 93-0192 at the AIAA 31st Aerospace Sciences Meeting and Exhibit, Reno, NV, Jan. 11–14, 1993; received Jan. 23, 1994; revision received March 28, 1994; accepted for publication March 28, 1994.

*Research Scientist, Fluid Mechanics Division, M/S 128. Member AIAA.

†Senior Research Scientist, Fluid Mechanics Division, M/S 128. Member AIAA.

Method

Computer Codes

CFL3D and TLNS3D both solve the three-dimensional time-dependent thin-layer Navier-Stokes equations with a finite-volume formulation. Both can employ grid sequencing, multigrid, and local time-stepping to accelerate convergence to steady state. When converged temporally to a steady-state solution, both methods are globally second-order accurate.

CFL3D, described in detail in Thomas et al.,[3] is an upwind code. For all results presented in this article, upwind-biased spatial differencing is used for the inviscid terms, and flux limiting is used to obtain smooth solutions in the vicinity of shock waves. All viscous terms are centrally differenced. The equations are solved implicitly with the use of three-factor approximate factorization (AF). Either Roe's flux difference splitting (FDS)[9] or van Leer's flux vector splitting (FVS)[10] can be employed to obtain fluxes at the cell faces.

TLNS3D, described in detail in Vatsa and Wedan,[4] is a central-difference code. Second-order central differences are used for all spatial derivatives, and a blend of second- and fourth-difference artificial dissipation terms is used to maintain numerical stability. These artificial dissipation terms can be added in either scalar or matrix form.[11] The solution is advanced explicitly in time using either a four- or five-stage Runge-Kutta time-marching algorithm.

Turbulence Models

Baldwin-Lomax

The Baldwin-Lomax (B-L) turbulence model[5] is used widely throughout the CFD community; its capabilities and limitations are well-known. In short, it is generally considered a good model for the prediction of attached flows, but it is deficient for flows with any significant separated regions. In particular, the B-L model tends to predict shocks too far downstream for separated transonic flows over aerodynamic configurations.

Johnson-King

The Johnson-King (J-K) turbulence model is a one-half equation turbulence model that requires the solution of an ordinary differential equation (ODE) over the body surface. Since its introduction,[6] several modifications and enhancements have been made.[12–15] Two different versions of the model will be described, as well as some of the effects of individual modifications. A more complete description of the evolution of these models can be found in Rumsey and Vatsa.[16]

In the "J-K1992" version of the model, so-called because of the date of the latest paper describing it,[15] the inner and outer models are given by

$$\mu_{t,i_{(\text{blend})}} = (1 - \Psi)\mu_{t,i_{(\text{eq})}} + \Psi\mu_{t,i_{(\text{J-K})}} \tag{1}$$

$$\mu_{t,0_{(\text{J-K})}} = 0.0168\rho q_\delta \delta^* \Gamma_{(\text{J-K})}\sigma \tag{2}$$

respectively, where

$$\mu_{t,i_{(\text{J-K})}} = 0.4\rho[D_{(\text{J-K})}]^2 y u_M \tag{3}$$

is the original Johnson-King inner-model formulation, $\mu_{t,i_{(\text{eq})}}$ is an equilibrium-type model, and

$$\Psi = \tanh[y(\tau_w^{1/2} + \tau_m^{1/2})/(y_m\tau_w^{1/2})] \tag{4}$$

Also

$$D_{(\text{J-K})} = 1 - \exp[-\rho_w y u_T/(A^+\mu_w)] \tag{5}$$

with A^+ taken as 17, and

$$\Gamma_{(\text{J-K})} = 1/[1 + 5.5(y/\delta)^6] \tag{6}$$

and u_T and u_M are the velocity scales

$$u_T = \max(u_M, \sqrt{\tau_w/\rho_w}) \tag{7}$$

$$u_M = (\sqrt{\rho_m/\rho})(\overline{-u'v'_m})^{1/2} \tag{8}$$

The term $\overline{-u'v'}$ represents the Reynolds shear stress ($=\tau/\rho$), q denotes total velocity, and the subscripts w and m denote wall value and value where $\overline{-u'v'}$ is maximum, respectively. The term σ is the modeling parameter that provides the link between the eddy-viscosity distribution and the rate equation for the development of $\overline{-u'v'_m}$. It will be described further below. The outer model [Eq. (2)] is simply the Clauser outer model, scaled by the parameter σ. The displacement thickness δ^* is computed by assuming that the boundary-layer edge is given by

$$\delta = 1.2y_{@\,(F/F_{\max}=0.5)} \tag{9}$$

Here, F is the Baldwin-Lomax parameter defined in Baldwin and Lomax.[5] A hyperbolic tangent (tanh) blending function is employed to merge the inner and outer models so that

$$\mu_t = \mu_{t,0_{(\text{J-K})}} \tanh[\mu_{t,i_{(\text{blend})}}/\mu_{t,0_{(\text{J-K})}}] \tag{10}$$

In the "J-K1990A" version of the model, developed by Abid et al.,[13] the inner model is given by Eq. (3) and the outer model is taken as the B-L expression, scaled by σ:

$$\mu_{t,0_{(1990\text{A})}} = (0.0168)(1.6)\rho F_{\text{wake}} F_{\text{kleb}}\sigma \tag{11}$$

where F_{wake} and F_{kleb} are defined in Baldwin and Lomax.[5] The velocity scale u_T is still given by Eq. (7), but u_M is taken as $(\overline{-u'v'_m})^{1/2}$. The blending between the inner and outer models is achieved with an exponential (exp) blending function:

$$\mu_t = \mu_{t,0_{(1990\text{A})}}\left\{1 - \exp\left[-\frac{\mu_{t,i_{(\text{J-K})}}}{\mu_{t,0_{(1990\text{A})}}}\right]\right\} \tag{12}$$

For both J-K1992 and J-K1990A, the rate equation governing the development of the maximum Reynolds shear stress is given by

$$\frac{D(\overline{-u'v'_m})}{Dt} = \frac{0.25}{L_M}(\overline{-u'v'_m}) \times [(\overline{-u'v'_{m,\text{eq}}})^{1/2} - (\overline{-u'v'_m})^{1/2}] - 0.25D_M \tag{13}$$

Here, the subscript eq denotes the equilibrium value of the maximum Reynolds shear stress, and L_M is taken to be $L_M = \min(0.4y_m, 0.09\delta)$. The turbulent diffusion term D_m is given by

$$D_M = \frac{0.5(\overline{-u'v'_m})^{3/2}\max(\sigma^{1/2} - 1, 0)}{0.25(0.7\delta - y_m)} \tag{14}$$

In this expression, the maximum (max) function allows the D_M term to contribute only in regions of flow recovery (where $\sigma > 1$). In the original model[6,12] the absolute value (abs) function was employed because it was erroneously assumed that D_M has negligible influence in regions where $\sigma < 1$. An additional benefit from using Eq. (14) is improved convergence for most transonic flow computations.

In CFL3D and TLNS3D, both the J-K1990A and J-K1992 versions of the Johnson-King turbulence model have been implemented. The Reynolds shear stress is assumed to be given by

$$\overline{-u'v'} = \mu_t\Omega/\rho \tag{15}$$

With the definition $g \equiv (\overline{-u'v'_m})^{-1/2}$, the rate Eq. (13) is reduced to a time-dependent linear equation that is solved using a multistage explicit Runge-Kutta time-stepping scheme for g, as described in Abid et al.[13] Boundary conditions for g at the trailing edge and at the transition trip are extrapolated from the computational domain, and symmetry conditions are employed on the side wall. The resulting value of g is then combined with the actual value of $\overline{-u'v'_m}$ in the flowfield to update σ via

$$\sigma^{t+\Delta t} = \sigma^t/(\overline{-u'v'_m}g^2) \tag{16}$$

at each step of an iteration process. The value of σ is limited in practice to lie between 0.1–4. In the J-K1992 model, the Prandtl-Van Driest formulation (i.e., the B-L inner model) is used for $\mu_{t,i_{(\text{eq})}}$ in Eq. (1). In wakes, both models revert to the B-L methodology. Transition is modeled by setting μ_t to zero along all of the grid lines that are normal to the wall within a preselected range.

The individual effects of some of the above-mentioned modifications to the J-K model on the shock location and extent of separation for two- and three-dimensional separated transonic flows (in the authors' experience) are listed in Table 1. The B-L outer-model expression generally produces higher

Table 1 Effect of modifications to J-K model

Shocks upstream (more separation)	Shocks downstream (less separation)
Clauser-type outer model	Baldwin-Lomax-type outer model
exp blending of inner and outer models	tanh blending of inner and outer models
abs function in diffusion term	max function in diffusion term
J-K inner model	Blended J-K/equilibrium inner model

eddy-viscosity levels than the Clauser model.[15] Hence, it tends to predict shocks further aft. For the same reason, the use of tanh-blending [Eq. (10)] generally yields shocks further downstream than exp-blending [Eq. (12)]. The final two modifications, the treatment of the turbulent diffusion term and the use of inner-model blending, tend to produce smaller effects than the first two. However, like all items in the table, these effects tend to be more pronounced for more-separated cases. The compressibility factor in Eq. (8) has little or no effect on transonic solutions.

Baldwin-Barth and Spalart-Allmaras

The Baldwin-Barth (B-B)[7] and Spalart-Allmaras (S-A)[8] turbulence models are both one-equation turbulence models for which a partial differential equation (PDE) is solved over the whole field. This PDE is solved implicitly using three-factor AF, with first-order upwind differencing used on the advective terms. Boundary conditions for the turbulence quantities are set such that the freestream μ_t is 0.9% that of μ_∞, symmetry conditions are employed on the side wall, and $\mu_t = 0$ on the body. The transition location is modeled by phasing out the source term along all of the grid lines that are normal to the wall within a preselected range.

Unlike both the B-L and J-K models, the B-B and S-A models lend themselves easily to programming on unstructured meshes because no inherent dependency on grid structure exists (e.g., there is no need to locate maximum values of quantities along grid lines normal to the wall). Also, no division into an inner and outer model, or into a wall and wake model, is made. Because they require the solution of a PDE over the whole flowfield at each time step, these models are more expensive than B-L or J-K; however, the solution to the PDE need not be converged fully at each time step for iteration toward a steady-state solution. The net result is an increase of less than 20% in CPU time over the B-L model.

Results

All airfoil cases are performed using the two-dimensional mode of CFL3D with FDS. The case chosen is case 10 from Cook et al.[17] for the RAE 2822 airfoil. The wind-tunnel corrections for case 10, taken from Baldwin and Barth,[7] are slightly different than those recommended in Cook et al. The primary grid used is a 257 × 97 C mesh with 177 points on the airfoil and a minimum spacing at the wall of $0.0000014c$ (where c represents chord). The outer boundary extent is approximately $15c$, and transition is assumed at 3% c. CFL3D solutions are run using a three-level multigrid algorithm. The l_2 norm of the residual of the equation for density generally converges three to four orders of magnitude in 400 cycles, although the lift generally reaches 0.5% of its steady-state value within 200–300 cycles. Typical times required on the Cray Y-MP computer for 400 cycles using a 257 × 97 grid are 214, 230, 249, and 254 CPU seconds for the B-L, J-K, B-B, and S-A models, respectively.

The conditions used for case 10 are $M = 0.75$, $\alpha = 2.72$ deg, and $Re = 6.2 \times 10^6$. Figures 1a and 1b compare the computed results using the B-L, J-K1992, J-K1990A, B-B, and S-A models to experimental results. The shock location is computed consistently by all models except B-L as slightly downstream of the experimental result. The B-L model predicts the shock location even further aft. Upstream of the shock, skin-friction coefficients are predicted consistently by B-L, J-K1992, B-B, and S-A, whereas J-K1990A yields levels that are low in comparison with the other models. Downstream of the shock, significant variation in skin friction levels exists between the models; in spite of this variation, J-K1990A again yields results that appear to be markedly different than results from the other models.

Although not visible in this figure, there is a small difference between the predicted shock locations using J-K1992 and J-K1990A (the latter is slightly further aft). However, this

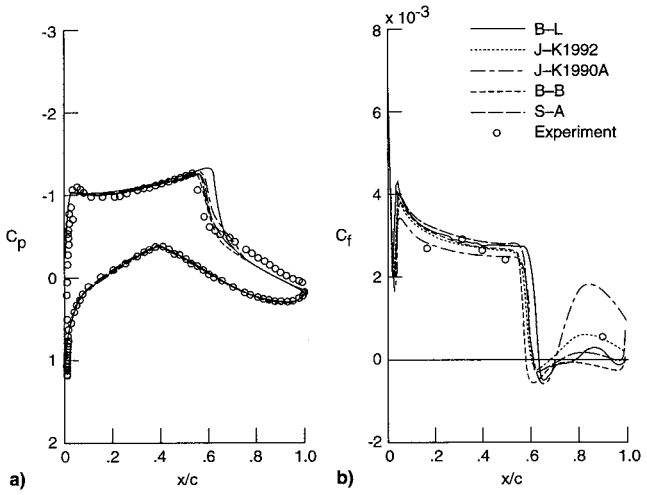

Fig. 1 Effect of turbulence model, RAE 2822 airfoil, $M = 0.75$, $\alpha = 2.72$ deg, $Re = 6.2 \times 10^6$, 257 × 97 grid, CFL3D.

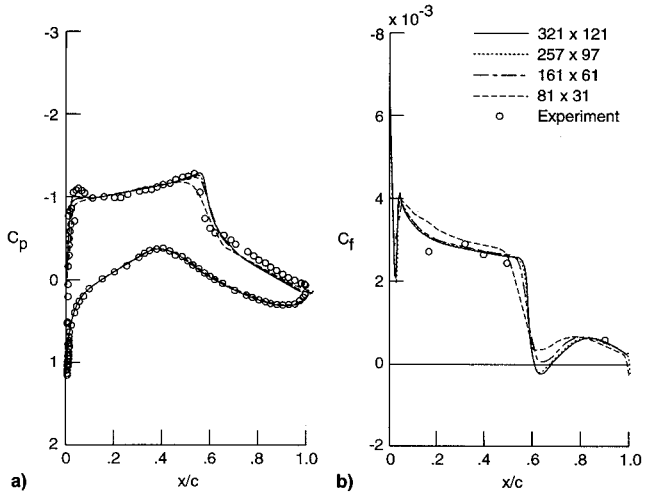

Fig. 2 Effect of grid density, RAE 2822 airfoil, $M = 0.75$, $\alpha = 2.72$ deg, $Re = 6.2 \times 10^6$, J-K1992 model, CFL3D.

difference is not as large as the difference reported in Johnson[15] between the J-K1992 model using the Clauser $\mu_{t,0}$ vs the B-L $\mu_{t,0}$. This disagreement is primarily due to the use of the exp blending in J-K1990A (as opposed to tanh blending), which partially counteracts the tendency of the B-L outer model to move shocks downstream. However, the use of exp blending is also the primary cause for the lower skin-friction levels in front of the shock using J-K1990A. The difference in skin friction behind the shock is attributable primarily to the different formulations of the inner model.

The effect of grid refinement on the computed results for the J-K1992 model is shown in Fig. 2. The surface pressure predictions do not differ significantly, as shown in Fig. 2a. In Fig. 2b, the skin friction decreases as the grid is refined, but the change is negligible between the two finer grids. The effect of grid refinement on results with the other turbulence models is similar.

Although not shown, surface pressure predictions for an attached-flow airfoil case (RAE 2822 case 9) using B-L, J-K1992, J-K1990A, B-B, and S-A are all fairly consistent, in reasonably good agreement with experimental data.

Both CFL3D and TLNS3D are used to compute three-dimensional flows over the ONERA M6 wing[1] and the Lockheed Wing C.[2] As recommended in Schmitt and Charpin,[1] no corrections to the wind-tunnel test conditions are employed for the ONERA M6 wing cases. For the Lockheed Wing C

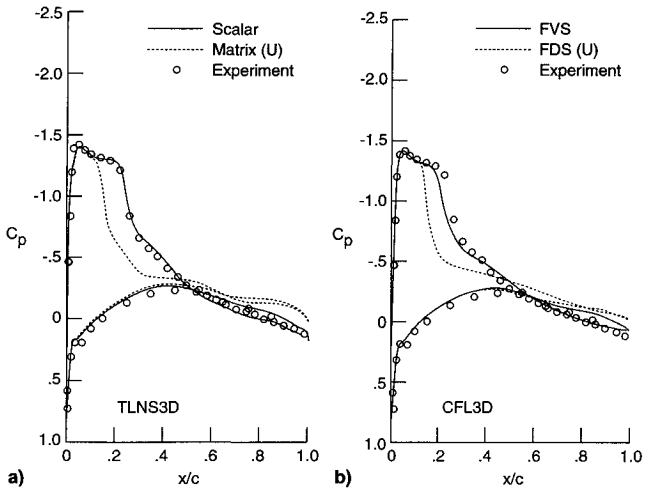

Fig. 3 Effect of dissipation levels, ONERA M6 wing, $M = 0.84$, $\alpha = 6.06$ deg, $Re_{mac} = 11.7 \times 10^6$, J-K1990A model, 193 × 49 × 33 grid, $2y/B = 0.90$. (*U*) indicates unsteady flow.

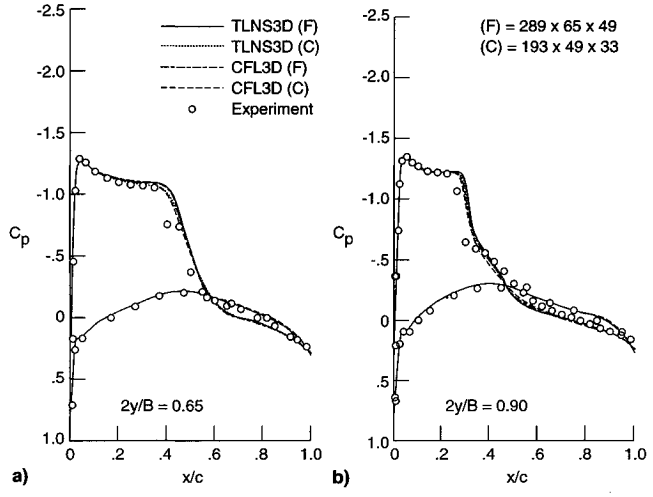

Fig. 4 Effect of grid and computer code, ONERA M6 wing, $M = 0.8447$, $\alpha = 5.06$ deg, $Re_{mac} = 11.7 \times 10^6$, J-K1990A model.

case, the corrections of Garriz et al.[18] are employed. For most of the ONERA M6 runs, a 193 × 49 × 33 C-O mesh is employed with 4785 points on the wing, a minimum normal spacing over the wing of $0.000015c_{root}$, and a distance from the wing to the outer boundary of at least $7.95c_{root}$. For the Lockheed Wing C calculations, a 241 × 49 × 49 C-O mesh is employed with 8673 points on the wing, a minimum normal spacing over the wing of $0.000001c_{root}$, and a distance from the wing to the outer boundary of at least $9.11c_{root}$. For all computations, transition is taken at approximately 3% *c*. Using a three-level multigrid strategy, both CFL3D and TLNS3D reduce the l_2 norm of $\Delta\rho$ by four to five orders of magnitude in 500 cycles for an ONERA M6 wing separated-flow case on a 193 × 49 × 33 grid. Typical times for each of the codes to reach 0.5% of final lift on this grid size is 1626 CPU seconds in 200 cycles for CFL3D and 1810 CPU seconds in 174 cycles for TLNS3D.

The first separated-flow case attempted is the $\alpha = 6.06$-deg case for the ONERA M6 wing, also reported in Abid et al.[13] The Mach number is $M = 0.84$ and $Re = 11.7 \times 10^6$ based on the mean aerodynamic chord. Using the J-K1990A model, the solution is found to vary extensively for TLNS3D and CFL3D, depending upon the levels of dissipation present. Figure 3a shows TLNS3D solutions at span station $2y/B = 0.90$ on a 193 × 49 × 33 grid with both scalar and matrix dissipation. (Trends at other span stations are similar.) The scalar dissipation case converges in excellent agreement with experimental results. However, lowering the dissipation levels gives unsteady, massive separation and moves the shock forward. [Note that the unsteady pressure distribution denoted by (*U*) in the figure is shown merely to indicate trends in the shock location prediction. Because the solution is not converged, these results do not portray any real physical behavior.] Although not shown, increasing the grid density to 289 × 65 × 49 using matrix dissipation still results in unsteady flow, while increasing the grid density using scalar dissipation results in very little change from the 193 × 49 × 33 scalar case. This lack of change by itself would suggest a grid-converged solution; however, with the solution using matrix dissipation in mind, this is clearly not the case because solutions using different dissipation levels should tend toward the same steady-state answer as the grid is refined.

CFL3D shows trends similar to TLNS3D, as shown in Fig. 3b. Here, the FVS scheme, which has more inherent dissipation than FDS, results in a steady-state solution with the shock position computed in good agreement with experimental results. However, the FDS solution is unsteady and massively separated. These computations indicate that either 1) at these conditions this wing is indeed massively separated and (probably) unsteady or 2) the ability of J-K1990A to accurately model the physics of the flow is dependent on the level of numerical dissipation present. These computations also demonstrate how easily one can be misled into thinking that a code is giving the "correct" answer, when in fact the truncation error has not been sufficiently reduced through grid-refinement and/or lowering dissipation levels.

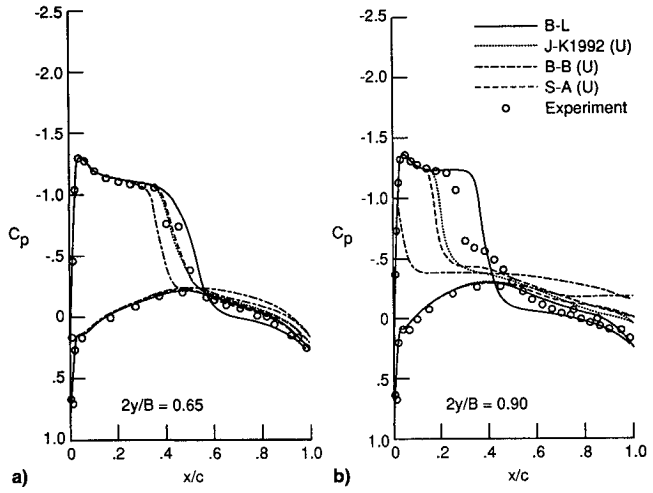

Fig. 5 Effect of turbulence model, ONERA M6 wing, $M = 0.8447$, $\alpha = 5.06$ deg, $Re_{mac} = 11.7 \times 10^6$, 193 × 49 × 33 grid, CFL3D. (*U*) indicates unsteady flow.

Because of questions regarding the nature of the ONERA M6 wing case for $\alpha = 6.06$ deg, comparisons are made instead at $\alpha = 5.06$ deg, for which shock-induced separation exists at a lesser extent. The Mach number for this case is $M = 0.8447$ and $Re_{mac} = 11.7 \times 10^6$. Figures 4a and 4b show the CFL3D and TLNS3D results on two different grids at two representative span stations, with the use of the J-K1990A model. As would be expected for grid-converged solutions, results on the two grids for both computer codes are almost the same. Although not shown, TLNS3D results with scalar dissipation and CFL3D results with FVS on the fine grid also give nearly the same results, which provides further evidence that grid convergence has been achieved for this case. The shock is generally predicted slightly downstream of experimental results.

Results using B-L, J-K1992, B-B, and S-A for the $\alpha = 5.06$-deg case are shown in Figs. 5a and 5b. The B-L model predicts the shock too far downstream in the region of the

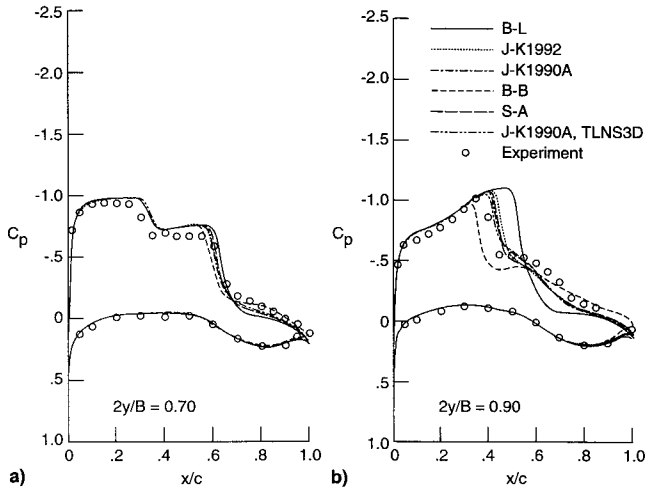

Fig. 6 Effect of turbulence model, Lockheed Wing C, $M = 0.8833$, $\alpha = 4.5$ deg, $Re_{mac} = 1 \times 10^7$, 241 × 49 × 49 grid.

wing where separation exists. The B-B, J-K1992, and S-A models all predict the shock too far upstream outboard of about $2y/B = 0.65$. TLNS3D with J-K1992 (not shown) shows similar behavior to CFL3D with J-K1992. Hence, for the Johnson-King turbulence model, better three-dimensional results for this case can be obtained using J-K1990A.

The separated-flow Lockheed Wing C case at the nominal conditions $M = 0.8999$, $\alpha = 4.91$ deg, and $Re_{mac} = 1 \times 10^7$ is run at the corrected conditions $M = 0.8833$, $\alpha = 4.5$ deg, and $Re_{mac} = 1 \times 10^7$. Computations are performed with CFL3D using five different turbulence models, as well as with TLNS3D using the J-K1990A model. All models yield converged steady-state results, which are shown in Figs. 6a and 6b at two span stations. At $2y/B = 0.7$, all turbulence models give roughly the same results, which are in good agreement with experimental results. However, near the wingtip, the B-L model predicts the shock too far aft, and the B-B model predicts it too far forward. All of the other models (including both J-K1992 and J-K1990A) yield consistent results that are in reasonable agreement with experimental results. TLNS3D and CFL3D results with J-K1990A are virtually the same.

Although not shown, surface pressure predictions for an attached-flow wing case (ONERA M6, $M = 0.84$, $\alpha = 3.06$ deg, and $Re_{mac} = 11.7 \times 10^6$) using B-L, J-K1992, J-K1990A, B-B, and S-A are all nearly the same, in good agreement with experimental data.

Conclusions

Four turbulence models have been evaluated for transonic two- and three-dimensional flows using the computer codes CFL3D and TLNS3D. In particular, two different versions of the Johnson-King model have been described and compared. The following observations about all of the turbulence models in general can be made:

1) The Baldwin-Lomax model works well for attached flows; however, shocks are predicted too far downstream for separated flows.

2) The Johnson-King model (version J-K1992), the Baldwin-Barth model, and the Spalart-Allmaras model work well for attached flows and two-dimensional separated flows, but can predict the shock too far upstream for some three-dimensional separated flows.

3) Version J-K1990A of the Johnson-King model generally predicts surface pressures for three-dimensional attached or separated flows very well, but does not work as well as version J-K1992 for two-dimensional flows (particularly in the prediction of skin friction).

Results of this investigation also indicate that excessive numerical truncation error can lead to an incorrect evaluation of turbulence models. Specifically, the use of scalar dissipation (as opposed to matrix dissipation) in a central-difference scheme, or the use of FVS (as opposed to FDS) in an upwind scheme, can alter the character of three-dimensional separated-flow solutions. By employing both central-difference and upwind computer codes to a given problem, in addition to performing grid sensitivity studies, this type of uncertainty can be minimized.

References

[1]Schmitt, V., and Charpin, F., "Pressure Distributions on the ONERA M6 Wing at Transonic Mach Numbers," AGARD AR-138, May 1979, p. B1.

[2]Hinson, B., and Burdges, K., "Acquisition and Application of Transonic Wing and Far-Field Test Data for Three-Dimensional Computational Method Evaluation, Volume II—Appendix B, Experimental Data," Air Force Office of Scientific Research, AFOSR-TR-80-0422, March 1980.

[3]Thomas, J., Krist, S., and Anderson, W., "Navier-Stokes Computations of Vortical Flows Over Low-Aspect-Ratio Wings," *AIAA Journal*, Vol. 28, No. 2, 1990, pp. 205–212.

[4]Vatsa, V., and Wedan, B., "Development of a Multigrid Code for 3-D Navier-Stokes Equations and Its Application to a Grid-Refinement Study," *Computers and Fluids*, Vol. 18, No. 4, 1990, pp. 391–403.

[5]Baldwin, B., and Lomax, H., "Thin Layer Approximation and Algebraic Model for Separated Turbulent Flow," AIAA Paper 78-257, Jan. 1978.

[6]Johnson, D., and King, L., "A Mathematically Simple Turbulence Closure Model for Attached and Separated Turbulent Boundary Layers," *AIAA Journal*, Vol. 23, No. 11, 1985, pp. 1684–1692.

[7]Baldwin, B., and Barth, T., "A One-Equation Turbulent Transport Model for High Reynolds Number Wall-Bounded Flows," NASA TM-102847, Aug. 1990.

[8]Spalart, P., and Allmaras, S., "A One-Equation Turbulence Model for Aerodynamic Flows," AIAA Paper 92-0439, Jan. 1992.

[9]Roe, P., "Approximate Riemann Solvers, Parameter Vectors, and Difference Schemes," *Journal of Computational Physics*, Vol. 43, No. 2, 1981, pp. 357–372.

[10]Van Leer, B., "Flux Vector Splitting for the Euler Equations," *Proceedings of the Eighth International Conference on Numerical Methods in Fluid Dynamics*, Lecture Notes in Physics, edited by E. Krause, Vol. 170, Springer-Verlag, Berlin, 1982, pp. 501–512.

[11]Turkel, E., and Vatsa, V., "Effect of Artificial Viscosity on Three-Dimensional Flow Solutions," *AIAA Journal*, Vol. 32, No. 1, 1994, pp. 39–45.

[12]Johnson, D., "Predictions of Transonic Separated Flow with an Eddy-Viscosity/Reynolds Shear Stress Closure Model," AIAA Paper 85-1683, July 1985.

[13]Abid, R., Vatsa, V., Johnson, D., and Wedan, B., "Prediction of Separated Transonic Wing Flows with Nonequilibrium Algebraic Turbulence Model," *AIAA Journal*, Vol. 28, No. 8, 1990, pp. 1426–1431.

[14]Johnson, D., and Coakley, T., "Improvements to a Nonequilibrium Algebraic Turbulence Model," *AIAA Journal*, Vol. 28, No. 11, 1990, pp. 2000–2003.

[15]Johnson, D., "Nonequilibrium Algebraic Turbulence Modeling Considerations for Transonic Airfoils and Wings," AIAA Paper 92-0026, Jan. 1992.

[16]Rumsey, C., and Vatsa, V., "A Comparison of the Predictive Capabilities of Several Turbulence Models Using Upwind and Central-Difference Computer Codes," AIAA Paper 93-0192, Jan. 1993.

[17]Cook, P., McDonald, M., and Firmin, M., "Airfoil RAE 2822—Pressure Distributions, and Boundary Layer Wake Measurements," AGARD AR-138, May 1979, p. A6.

[18]Garriz, J., Newman, P., Vatsa, V., Haigler, K., and Burdges, K., "Evaluation of Transonic Wall Interference Assessment and Corrections for Semi-Span Wing Data," AIAA Paper 90-1433, June 1990.